Discrete Modal Decomposition: a new approach for the reflectance modeling and rendering of real surfaces

Gilles Pitard, Gaëtan Le Goïc, Alamin Mansouri, Hugues Favrelière, Simon-Frédéric Desage, Serge Samper, Maurice Pillet

Discrete Modal Decomposition: a new approach for the reflectance modeling and rendering of real surfaces

Gilles Pitard[1] · Gaëtan Le Goïc[2] · Alamin Mansouri[2] · Hugues Favrelière[1] · Simon-Frederic Desage[1] · Serge Samper[1] · Maurice Pillet[1]

Abstract Reflectance Transformation Imaging is a recent technique allowing for the measurement and the modeling of one of the most influential parameters on the appearance of a surface, namely the angular reflectance, thanks to the change in the direction of the lighting during acquisition. From these photometric stereo images (discrete data), the angular reflectance is modeled to allow both interactive and continuous relighting of the inspected surface. Two families of functions, based on polynomials and on hemispherical harmonics, are cited and used in the literature at this aim, respectively, associated to the PTM and HSH techniques. In this paper, we propose a novel method called Discrete Modal Decomposition (DMD) based on a particular and appropriate Eigen basis derived from a structural dynamic problem. The performance of the proposed method is compared with the PTM and HSH results on three real surfaces showing different reflection behaviors. Comparisons are made in terms of both visual rendering and of statistical error (local and global). The obtained results show that the DMD is more efficient in that it allows for a more accurate modeling of the angular reflectance when light–matter interaction is complex such as the presence of shadows, specularities and inter-reflections.

Keywords Surface visual appearance · Reflectance modeling and rendering · RTI · Image relighting · Discrete Modal Decomposition · Quality inspection

✉ Gilles Pitard
pitard.gilles@gmail.com

[1] Laboratoire SYMME, EA 4144, Univ. Savoie Mont Blanc, Annecy, France

[2] Laboratoire LE2I, FRE2005 CNRS ENSAM, Univ. Bourgogne Franche-Comté, Auxerre, France

1 Introduction

The measurement and modeling of the surface appearance is an important challenge at both scientific and application levels, such as quality inspection and controlling the manufacturing process in industry (aerospace, automotive, packaging, jewelry, cosmetics) or documentation of cultural heritage artifacts. Beside, on the one hand, the visual perception of surfaces is an unconscious and complex mental processing influenced both by the perception-based representations of past experiences and by the ongoing tasks. On the other hand, visual appearance is also related to the resulting sensory responses of measurable physical stimuli by means of adequate instruments. The choice of measuring instrument therefore requires a sound understanding of the multi-physical interactions (light, material, surface roughness, reflectance, etc.) involved in the perception of surfaces.

Two main approaches are possible to address this issue. The first is *geometric* in that it aims to model the visual behavior of a surface from its 3D measurement. Results in the field of surface topography [1–3] show that the correlations between 3D roughness parameters and surface appearance remain difficult to establish, particularly in the case of real surfaces [4], where visual behaviors are locally heterogeneous and often require a multi-scale analysis. Moreover, the acquisition of topographical data is often point-wise leading to a huge amount of data, which are time-consuming for processing and analysis. The second approach is *photometric*: the modeling of the visual behavior is directly based on the photometric measurement of the light reflection on the inspected surface. The most comprehensive technique is the estimation of the Bidirectional Reflectance Distribution Function (BRDF) [5,6] on each point of the inspected surface. However, a conventional

BRDF measurement is inappropriate in many application contexts such as the inspection of visually salient anomalies on real surfaces. Such approach is indeed time-consuming: a sparse sampling of both the incident light and the reflection domain implies to manage large volumes of data and typically induces several hours of acquisition in very constrained conditions. Methods based on simplification of the global model of BRDF to its components deemed most pertinent have then been developed. For instance, techniques known as Bidirectional Texture Function [7–9] provide a texture image that enables to synthesize surface appearance under all illumination and viewing directions (image relighting). Malzbender et al. [10–12] proposed a simplified formulation of the BTF approach by holding the photometric sensor in a fixed position (a camera is generally fixed vertically to the inspected surface). This technique is called Reflectance Transformation Imaging techniques (RTI) and the associated method for relighting is called Polynomial Texture Mappings. The setup and method proposed in this paper for measuring and modeling the visual appearance of real surfaces fall within the scope of these techniques.

In the RTI acquisition process, the view point and the distance from the camera to the objects are fixed, only the lighting directions (generally 30–100 directions) in the incident light domain vary. For each lighting direction an image is acquired. From these discrete data, also called photometric stereo acquisitions, an angular reflectance function is locally estimated at each pixel, allowing after reconstruction the interactive relighting of the surface. In addition, this modality of acquisition makes possible to assess geometrical descriptors on the inspected surface, such as local directional slopes and curvatures, and even 3D reconstruction of surfaces by integration of the normal field information [13,14]. Two reconstruction methods also called parametrizations are generally used to model the angular reflectance, based on polynomials [10] and hemispherical harmonics [15], and named, respectively, PTM and HSH. Although the HSH method improves the reliability of the description of the angular reflectance of surfaces [16,17], it remains insufficient in the case of complex surfaces (non-Lambertian behaviors) characterized by an oversmoothing of the angular reflectance variations due to the presence of specularities, as depicted in Fig. 6 for instance. Therefore, we propose a new parametrization aiming at more reliable reconstruction of the appearance of real surfaces. After having introduced existing methods and related works in Sect. 3, this new technique called Discrete Modal Decomposition (DMD) is described in Sect. 4. The method is applied on three surfaces from industry and cultural heritage, and results are compared with the conventional PTM and HSH techniques (Sect. 5) before concluding.

2 Measuring surface appearance

2.1 Approach

As indicated before, the relevant photometric quantity for measuring the appearance is the BRDF since it characterizes in a comprehensive manner the distribution of the light reflected from a surface, in angular and spectral terms [18–20]. In terms of human perception, the reflectance is interpreted by the human visual system at different spatial scales in order to extract relevant parameters, as the size and shape of the specular lobe, and appreciate the appearance of the observed surface, such as the regularity of texture, the uniformity of color, the gloss, or the criticity of appearance anomalies. The multi-scale acquisition carried out by the human visual system is hardly reproducible by an automatic instrumental device for tasks like inspection and/or digitization a lot of real surfaces. A solution to reduce the amount of information consists then to supplement the data by a reflectance analytical model. Different models were thus used depending on the approach (empirical, geometric or physical), associated with different scales. We can cite Lambert, Phong and Blinn [21] (taking into account the specular term), Lafortune (cosinusoidal functions) [22], Ward (Gaussian lobes) [23], Schröder et Sweldens (spherical wavelets) [24], Koenderink (Zernike polynomials) [25]. In addition to optical models, various geometric ones have also been developed, such as Cook and Torrance [26], Oren and Nayar [27], Beckmann and Spizzichino [28], or He [29] model, which differ mainly in terms of both the quantity used to model surface variation (amplitudes, slopes) and of the distribution function (Gaussian, Lorentzian, etc.). The microfacet models are now common in applications related to the reconstruction of the appearance of virtual surfaces, but often imply a strong assumption on texture homogeneity. Though refining these reflection models by integrating the data of measurements on real surfaces can be relevant [21,30,31], the analytical BRDF models are not appropriate for the specific task of inspection and more generally for the modeling of real surfaces. Other BRDF-reduction models have also been proposed, as for example the light transport method approaches. They demonstrate very interesting performances for image relighting with complex light behaviors such as caustics, complex occlusions or sub-surface scattering [32,33]. However, the reflectance acquisition process, made punctually on the inspected surface, is still time-consuming (approximately 2 h for a 1.5 Mp image) [34], and make not possible its implementation for applications such as the inspection of the appearance behavior/quality of real surfaces.

On the other side, inverse modeling (fitting a model to data) is widely employed in surface problems for data com-

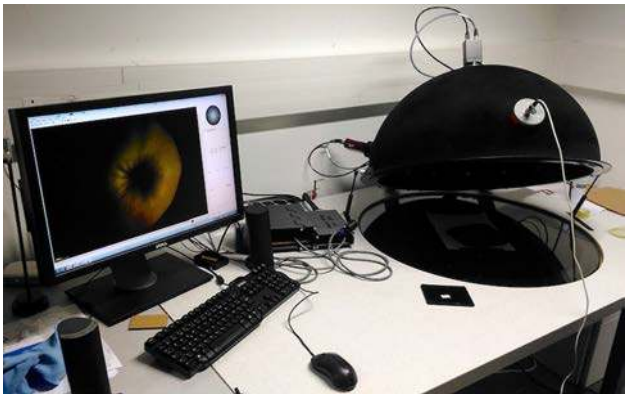

Fig. 1 Multi-view RTI setup called *"MeSurA Sphere"*

paction and processing/rendering speed-up. One of the most efficient techniques in this context is the RTI [35,36] technique. From the acquired discrete RTI data (set of images), a continuous model of angular reflectance can then be estimated at each point of the inspected surface. The original method, called Polynomial Texture Mappings, uses a basis of polynomial functions to compute this inverse modeling [10–12,37]. This PTM model as well as the HSH show quite realistic rendering but fail in the presence of complex reflectances (as non-Lambertian behaviors) and leads to an oversmoothing of the local angular reflectances. To address this issue, i.e., in order to perform an accurate reflectance reconstruction, we developed and implemented a setup along with a model based on a non-orthogonal projection derived from dynamics, called Discrete Modal Decomposition.

2.2 Angular reflectance acquisition setup

The proposed approach implies the acquisition of photometric stereo data, i.e., the acquisition of a set of images from a fixed position of the camera, at constant exposure, while varying the light incidence at each shot. The light sources are distributed uniformly over the incident light domain, to cover a wide range of angles of colatitude θ and of azimuth ϕ. Malzbender originally used a rigid opaque dome [11] with a single camera placed orthogonal to the studied surface, and adjustable in relation to the type and the size of the objects to acquire (focal length, depth of field,…). In the fields of archeology and historical artifact conservation [38–41], the intrinsic constraints of the object and its environment make manual acquisition protocol necessary. Other devices control a motorized arc using one or more light sources placed around the object. In each case, the viewing angle (camera position) is fixed, which turns to be limited in the case of inspection of certain complex shapes, such as revolution or freeform surfaces, requiring several viewing angles.

For the particular case of quality inspection of small objects, we designed a multi-view device called *"MeSurA Sphere"* (Fig. 1). The general architecture is shown in

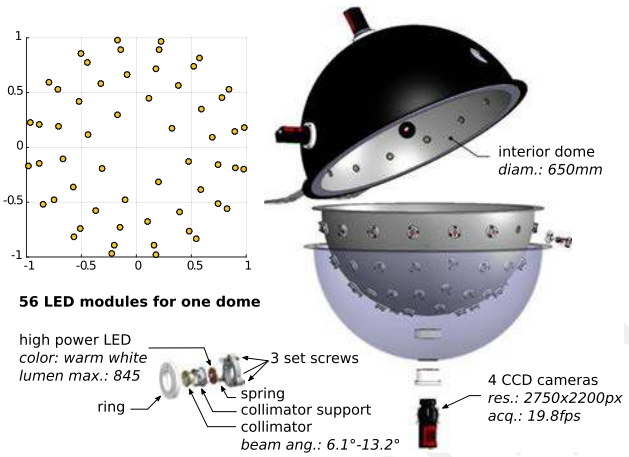

Fig. 2 Architecture of the MeSurA Sphere: a multi-view photometric stereo setup

Fig. 2. This device uses the principles of RTI acquisition described by Malzbender and formed by two opaque domes on which white light sources are distributed (high-power LED, 4500 K). Several improvements were made in order to provide solutions to the limitations of the existing RTI devices and meet industrial requirements:

- Multiple fixed points of view were spread over a sphere instead of the more conventional half-sphere, this will allow for the simultaneous acquisition of the scene from different angles and thus analyze complex surface structures without touching the object under inspection. In terms of processing, this RTI multi-view system opens up perspectives for a combination of 3D reconstruction modalities (stereovision) with the acquisition of photometric stereo information (modeling and simulation of appearance, estimation of slope and curvature).
- Controlling the direction of light sources onto the dome or sphere is essential to the quality of the information acquired although this factor is often under-controlled in existing systems (potential errors related to sphere shape deviations, to the fixing systems of the sources on the dome,…). We have allowed for the individual adjustment in direction of each LED to $\pm 0.1°$ and re-calibration of the device used, if necessary using a referencing machine. This mechanical device which maintains each of the light sources in position can also optimize natural cooling (air) of the light sources.
- Taking into account the context referred to for this work (industrial visual quality inspection), important development work was done on the aspects relating to its automation and acquisition time reduction: acquisition, transfer and processing times are significantly reduced by suitable hardware choices (high-speed cameras and GigE Ethernet interface devices) and the use of versatile and multifunctional softwares.

We implemented our method on a PC with Intel Core i7 3.40 GHz CPU and 16 GB of memory. In our implementation, we can capture a set of 56 × 2 images (for 2 domes) of the inspected surface from three different camera positions, with a 6 Mp resolution in approximately 30 s. A typical acquisition session including the image acquisition and the angular reflectance estimation on each point/pixel of the inspected surface using the DMD modeling approach takes about 3 min. A particular strength of the method resides in the ability to reconstruct the rendering (relighting) in a chosen direction instantly once the calculation of the DMD coefficients has been completed. This allows a truly interactive rendering/relighting, as required for visual surface inspection tasks.

3 Background and related works

3.1 Problem formulation

A photometric stereo acquisition setup is used to obtain a set of luminance values associated with acquisition light directions. From this discrete luminance information, the principle of the method consists in estimating in each pixel (x, y) of the inspected surface an angular reflectance function which describes the amount of light re-emitted by the surface in the direction of the photometric sensor system, as a function of the light direction angles. The estimated intensity I_{meas} in each pixel can thus be expressed by Eq. 1, where θ and ϕ are the angles associated with the lighting direction, respectively, the colatitude and the azimuth.

$$I_{\text{meas}} = I_{r,g,b}(\theta, \phi, x, y) = L(\theta, \phi, x, y) C_{r,g,b}(x, y) \quad (1)$$

where L and C represent the luminance and the chromaticity information for the (x, y) pixel. The term C does not depend on the angles (θ, ϕ) because the chromaticity variation potentially induced by the change of light direction is not taken into account for this kind of approach. Moreover, the functions of angular reflectance are expressed within the framework of the RTI technique in the local coordinate system (l_u, l_v). This coordinate system is associated with the projection of the direction vector $\overrightarrow{u_e(\theta, \phi)}$ in the horizontal plane. Thus, the angles (θ, ϕ) can be expressed by:

$$\theta = \arccos\left(\sqrt{1 - l_u^2 - l_v^2}\right) \text{ and } \phi = \arctan 2(l_u, l_v) \quad (2)$$

The encoded gray level $\mathcal{G}$ by the camera of a pixel is directly proportional to the luminance $L(\overrightarrow{u_c})$ in the direction of the optical center [42], provided that an appropriate calibration of the photometric device is performed. This model could be extended to take into account some nonlinearities [43], linked for example to shadows, overexposures or multi-reflection phenomena. We can then express the gray level measured in each pixel by Eq. 3 where k is the proportionality factor that may vary depending of the used camera (linearity, gain, transmission factor of lenses,…).

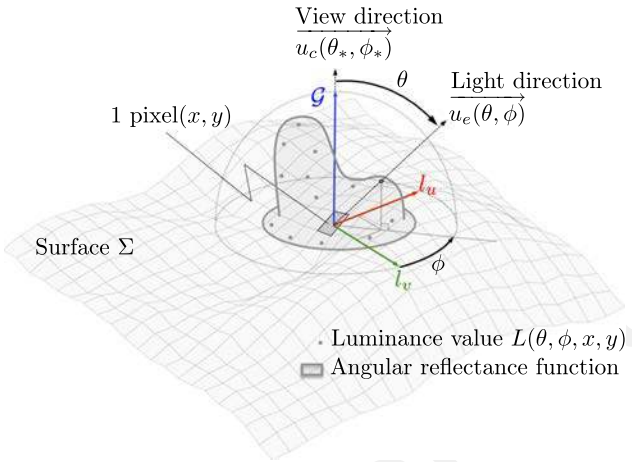

Fig. 3 Geometric configuration (camera-surface-light source) allowing the acquisition and the parametrization of the angular reflectance function from the measured values of luminance at one pixel (x, y)

$$\mathcal{G} = k \times g \quad with \quad g = L(\overrightarrow{u_c}) = L(l_u, l_v, x, y) \quad (3)$$

Figure 3 shows, for pixel coordinates (x, y), the angular reflectance function estimated from different directions of illumination (θ_i, ϕ_i) while the image acquisition process is performed. The camera is fixed (θ_*, ϕ_*). The estimated local angular reflectance function is represented in the spatial coordinate system (l_u, l_v).

3.2 Related works

Different types of functions can be used for the parametrization of the angular component of reflectance. In this section, we describe the two popular approaches named PTM and HSH and, respectively, based on polynomial functions (PTM) and on a linear combination of hemispherical harmonics.

3.2.1 Polynomial Texture Mapping (PTM)

This technique was developed by Malzbender et al. [10–12] with the aim of improving photo-realistic rendering. Angular polynomial parametrization of reflectance is described in [44] where through the use of Eq. 4, information on each pixel is described.

$$L(l_u, l_v) = a_0 + a_1 l_u + a_2 l_v + a_3 l_u l_v + a_4 l_u^2 + a_5 l_v^2 \quad (4)$$

The calculation of the polynomial coefficients $(a_0 - a_5)$ is carried out by an approximation of the point cloud associated

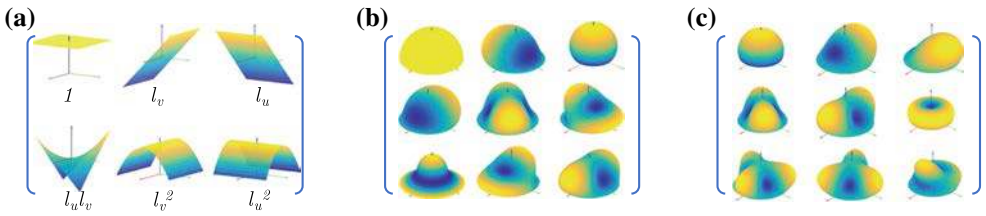

Fig. 4 Representation of the angular reflectance description functions **a** second-order polynomials, **b** hemispherical harmonics (9 first descriptors) and **c** reflectance Modal Basis (9 first descriptors)

with luminance measured for each pixel (multiple regression system of Eq. 5) and corresponds to a discrete projection of the luminance in the polynomial function basis of order 2 as illustrated in Fig. 4a.

$$\begin{bmatrix} l_{u0}^2 & l_{v0}^2 & l_{u0}l_{v0} & l_{u0} & l_{v0} & 1 \\ l_{u1}^2 & l_{v1}^2 & l_{u1}l_{v1} & l_{u1} & l_{v1} & 1 \\ . & . & . & . & . & . \\ . & . & . & . & . & . \\ . & . & . & . & . & . \\ l_{uN}^2 & l_{vN}^2 & l_{uN}l_{vN} & l_{uN} & l_{vN} & 1 \end{bmatrix} \begin{bmatrix} a_5 \\ a_4 \\ a_3 \\ a_2 \\ a_1 \\ a_0 \end{bmatrix} = \begin{bmatrix} L_0 \\ L_1 \\ . \\ . \\ . \\ L_N \end{bmatrix} \tag{5}$$

Once the six polynomial coefficients ($a_0 - a_5$) are calculated, they are used to simulate the appearance of the studied surface (on each pixel) under any illumination direction, almost instantaneously. The six polynomial projection descriptors presented in Fig. 4a correspond to a mode of translation, two modes of inclination, a saddle-shaped mode and two parabolic modes. The complexity reachable in combining these basic shapes is reduced and leads to oversmoothing when rapid changes of reflectance occur (Fig. 6a), due to shadows, specularities, or inter-reflections.

3.2.2 Hemispherical harmonics (HSH)

This technique [15,16] is an improvement in the PTM approach implementing a projection space based on hemispherical harmonics (HSH) noted $H_l^m(\theta, \phi)$, where l is the order and m the degree. These functions are derived from shifted Associated Legendre Polynomials (ALPs) over the interval $x \in [0, 1]$ using the linear transformation of x to $2x - 1$ (Eq. 6).

$$\tilde{P}_l^m(x) = P_l^m(2x - 1) \tag{6}$$

This shift in spherical harmonics domain to the half-space formed by the hemispheric functions allows for a reduction to the domain in which the BRDF function is expressed. By replacing x by $cos(\theta)$ in Eq. 6, we get defined polynomials over the angular interval $\theta = [0, \pi/2]$ corresponding to the values taken by the polar angle on the hemisphere. Legendre's polynomials P_l^m can be computed efficiently using recurrence relations [15]. The Hemispherical Harmonics $H_l^m(\theta, \phi)$ are thereby expressed:

$$H_l^m(\theta, \phi) = \begin{cases} \sqrt{2}\tilde{K}_l^m \cos(m\phi)\tilde{P}_l^m(\cos\theta) & (m > 0) \\ \sqrt{2}\tilde{K}_l^m \sin(-m\phi)\tilde{P}_l^{-m}(\cos\theta) & (m < 0) \\ \tilde{K}_l^0 \tilde{P}_l^0(\cos\theta) & (m = 0) \end{cases} \tag{7}$$

with the following value of normalization $\tilde{K}_l^m$:

$$\tilde{K}_l^m = \sqrt{\frac{(2l+1)(l-|m|)!}{2\pi(l+|m|)!}} \tag{8}$$

Any function describing surface reflectance can then be decomposed into a series of HSHs [36,45–48], of order l and degree m (Eq. 9a), where coefficients (contributions) C_l^m are obtained by projection of reflectance function f in the space of the hemispherical harmonic functions (Eq. 9b):

$$f_{(\theta_v,\phi_v)}(\theta_i, \phi_i) = \sum_{l=0}^{n} \sum_{m=-l}^{l} C_l^m(\theta_v, \phi_v) H_l^m(\theta_i, \phi_i) + R_n \tag{9a}$$

$$C_l^m(\theta_v, \phi_v) = \int_0^{2\pi} \int_0^{\frac{\pi}{2}} f(\theta_v, \phi_v, \theta_i, \phi_i) H_l^m(\theta_i, \phi_i) \sin\theta_i d\theta_i d\phi_i \tag{9b}$$

4 Proposed method

A new projection basis, namely the Discrete Modal Decomposition (DMD), is proposed to estimate the angular reflectance function on each pixel of the inspected surface from stereo photometric images. Similar to a discrete Fourier transform, this decomposition allows one to evaluate the spectral content of a discrete signal, from a projection basis consisting of vectors resulting from a structural dynamics problem. DMD has notably been developed and applied for characterization and specification of geometric deviations in form in the field of geometric tolerancing [49,50], the 3D multi-scale topographic measurements of roughness analysis [51,52], or even for the estimation of spatial term of

a heat diffusion problem [53,54]. Results show that this non-orthogonal projection basis not only provides closer assessment of the estimated information (3D shape, roughness, heat source spatial term) but is also more robust against noise and side effects. In the current context with regard to angular reflectance modeling, the objective is to enable a more accurate description of the local angular reflectance functions on each point/pixel of surfaces emanating from real objects (i.e., non-virtual, showing spatial heterogeneities and complex reflectance behaviors).

4.1 Modal basis and decomposition

Depending on the applications and the data to parametrize, modal decomposition can be implemented with different sets of vectors, called modal basis. The choice of the type and construction parameters of the decomposition basis (notably the boundary conditions) is crucial for an efficient decomposition [53] (good approximation with minimum number of descriptors). To implement the DMD for the purpose of the angular component of reflectance reconstruction, we chose to build a basis, called Reflectance Modal Basis (RMB), drawn from a hemispheric reference surface that physically corresponds to an ideal Lambertian surface. Concerning the formulation of the boundary conditions, it was chosen to impose no-inplane displacement on the base circle of the hemispherical surface. This choice helps to obtain a more efficient basis for complex reflectance surface morphologies. The construction stages of the RMB are described below, and a representation of the geometric functions used for the modeling of the angular reflectance information is presented in Fig. 4 (PTM, HSH and DMD basis). For the HSH and DMD basis, these representations describe the deviations from an hemispherical reference form, that can be associated physically to a Lambertian angular reflectance behavior.

The associated geometry (the hemispherical surface) leads to the definition of the dynamic structural problem described by Eq. 10a, where M and K are the matrices of mass and stiffness, θ, ϕ and t are, respectively, the angles associated to the light direction and the time variable. Under such formalism, $q = q(\theta, \phi, t)$ stands for the displacements which characterize the modal shapes. Such a problem classically gives the frequency-based solution expressed in Eq. 10b, where Q_k is the vector of amplitude associated with the pulsation w_k.

$$M.\ddot{q} + K.q = 0 \quad with \quad q = q(\theta, \phi, t) \tag{10a}$$

$$q(\theta, \phi, t) = \sum_{k=1}^{+\infty} Q_k \cos(w_k t) \tag{10b}$$

Modes defined by (Q_k, w_k) are determined by solving the linear system (Eq. 11), where I is the identity matrix, and $M^{-1}K$ is assumed to be diagonalizable. The discrete solution is computed by a Finite Element Analysis (FEA) and provides the basis of projection named the RMB $(Q_1 \ldots, Q_n)$, where n is the number of calculated modes.

$$\left(M^{-1}K - \frac{1}{w_k^2} I\right) Q_k = 0 \tag{11}$$

4.2 DMD-based reflectance modeling (RMB)

For each pixel, the angular reflectance function f can then be expressed as a linear combination of modal vectors and the residue of decomposition R_n (Eq. 12a), where the modal coefficients λ_k are obtained by the projection of the vector of measured luminances L onto each of the basis modes. However, as the modal basis is not orthonormal, the classic projection operator $P_Q = QQ^T$ cannot be used. Indeed, the use of the dual basis $Q^* = (Q^T Q)^{-1} Q^T$ is required. An infinity norm is assigned to modal vectors such as $||Q_k||_\infty = 1$. All of the resulting modal coefficients resulting from the projection of luminance values L in the non-orthonormal modal projection basis is expressed by Eq. 12b.

$$f_{(\theta_v,\phi_v)}(\theta_i, \phi_i) = \sum_{k=1}^{n} \lambda_k(\theta_v, \phi_v) Q_k(\theta_i, \phi_i) + R_n \tag{12a}$$

$$\lambda_k(\theta_v, \phi_v) = (Q_k{}^T Q_k)^{-1} Q_k{}^T.L \tag{12b}$$

Summarily, the modal parametrization is an adaptive method, both in terms of type and the construction hypotheses for the set of decomposition vectors and in terms of the number of modes. Indeed in practice, one adjusts the number of descriptors depending on the density of the acquisitions (chosen according to the Nyquist–Shannon Sampling Theorem), the complexity of the shape of the surfaces potentially described going up when n increases. Figure 6c shows surface reflectance approximated by DMD, compared to other projection bases (PTM, HSH).

5 Experiments, assessment and results

In this section, we present an evaluation of the proposed approach. First, datasets from the RTI acquisitions used are described. Then, the results of reconstruction using DMD are compared to those using PTM and HSH. This comparison is also made by visual evaluation in terms of pixel-to-pixel differences and local and global maps.

5.1 Datasets

The application of the modal approach for the modeling of appearance, as well as comparison with results from the PTM

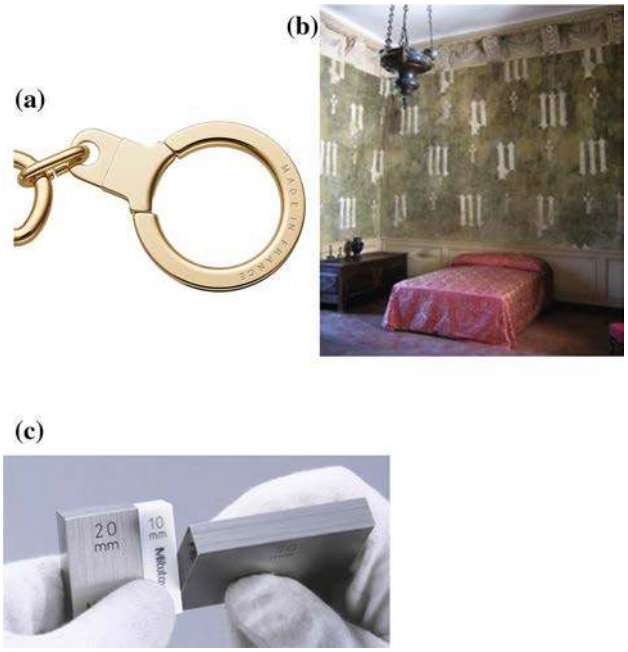

Fig. 5 Sample of surfaces selected for *Dataset* 1−3. **a** Ring of jewelry (*Dataset 1*), **b** wall paintings at the *Château de Germolles* and **c** gauge block (unidirectional brushed pattern)

and HSH methods, is performed on three representative surfaces. These three surfaces were chosen because of their significant difference regarding the luminous behavior allowing hence a thorough assessment of the performance of the three methods.

Dataset 1. This sample is a piece of gold-plated jewelry, having the shape of a ring (Fig. 5a) and whose surface is mirror-polished. The surface exhibits several local specularities, due to the presence of a variety of local defects such as scratches or pinholes. The associated problem in this case study particularly concerns the detection and analysis of local visual anomalies, and more generally the inspection of the visual quality of the shiny surfaces. The outside diameter of the ring is about 40 mm.

Like this sample, many industrial surfaces are metal surfaces in which the gloss aspect is obtained on the surface using different finishing operations (brushing, sanding, polishing, etc.). Undesired alterations related to the manufacturing process or manipulation of objects can produce a variety of anomalies on these surfaces. The modeling of these phenomena requires an accurate description of complex local shapes of reflectance.

Dataset 2. This RTI acquisition set was acquired from a portion of historical wall painting of the *Château de Germolles* (Fig. 5b), which is a non-documented restoration project and that raises certain questions [55]. Among the raised issues, we can cite the stratigraphy, to origin of the green color and also the brush marks on the boundaries of the letters "P" and "M". The presence of gold and tin is also suspected.

Light behavior here is more Lambertian than for the sample *Dataset* 1, since the visual aspect of this painting is generally diffuse. However, the presence of local relief (gold and tin) due to retouching on the heterogeneous surface induce significant spatial variations in reflectance on the surface of the analyzed area. In terms of scale, this area represents approximately 10 cm^2.

Dataset 3. This sample is a gauge block used as a standard reference to check the calibration of measurement tools. The manufacture of gauge blocks implies lapping and polishing processes with high precision for achieving a fine surface finish. These gauges have to be of very high quality (precision and location of patterns) which requires a strong quality control stage (anomaly detection). One of the sides of the gauge block has an unidirectional brushed pattern.

5.2 Comparison with PTM and HSH

The first step in exploiting the RTI acquisition data is the approximation of the points cloud obtained—representing discrete measurements of reflectance—by the optimal continuous function of the data. This reconstruction is shown in Fig. 6. We can appreciate the quality of the reconstruction obtained by these different methods; PTM, HSH and

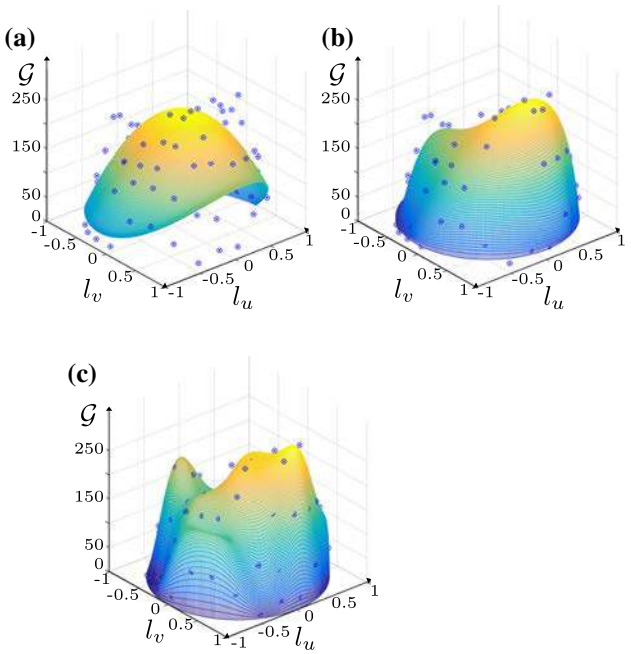

Fig. 6 Reflectance surface approximated of one pixel (x, y) from *Dataset* 1. **a** PTM (2nd degree polynomials), **b** HSH (2nd order hemispherical harmonics) and **c** DMD (Discrete Modal Decomposition)

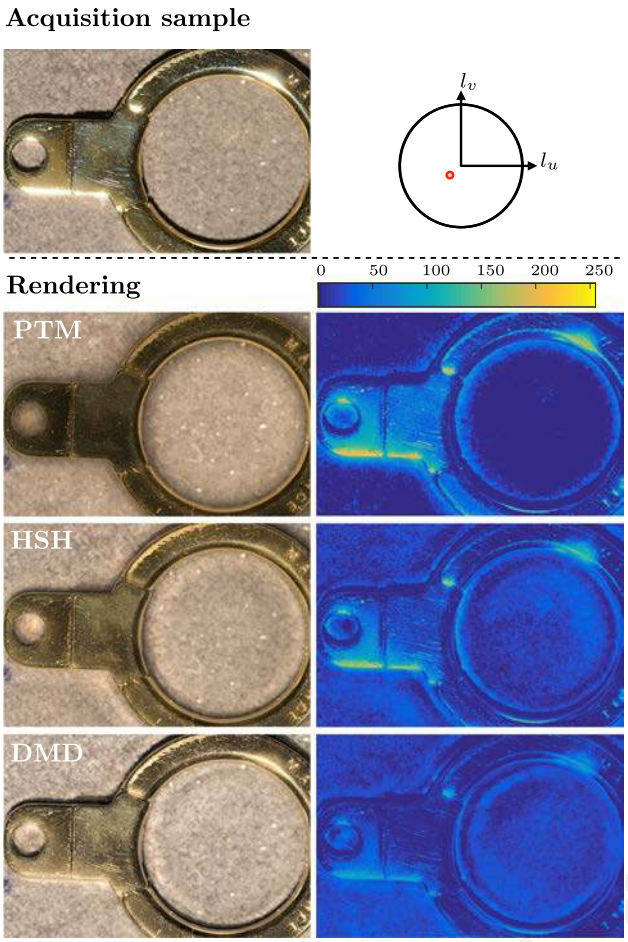

Fig. 7 Macroscopic views of the acquired and reconstructed images from *Dataset* 1, in a single direction of illumination, by the *PTM*, *HSH* and *DMD* methods (*left-side*), with the associated error maps (*right-side*)

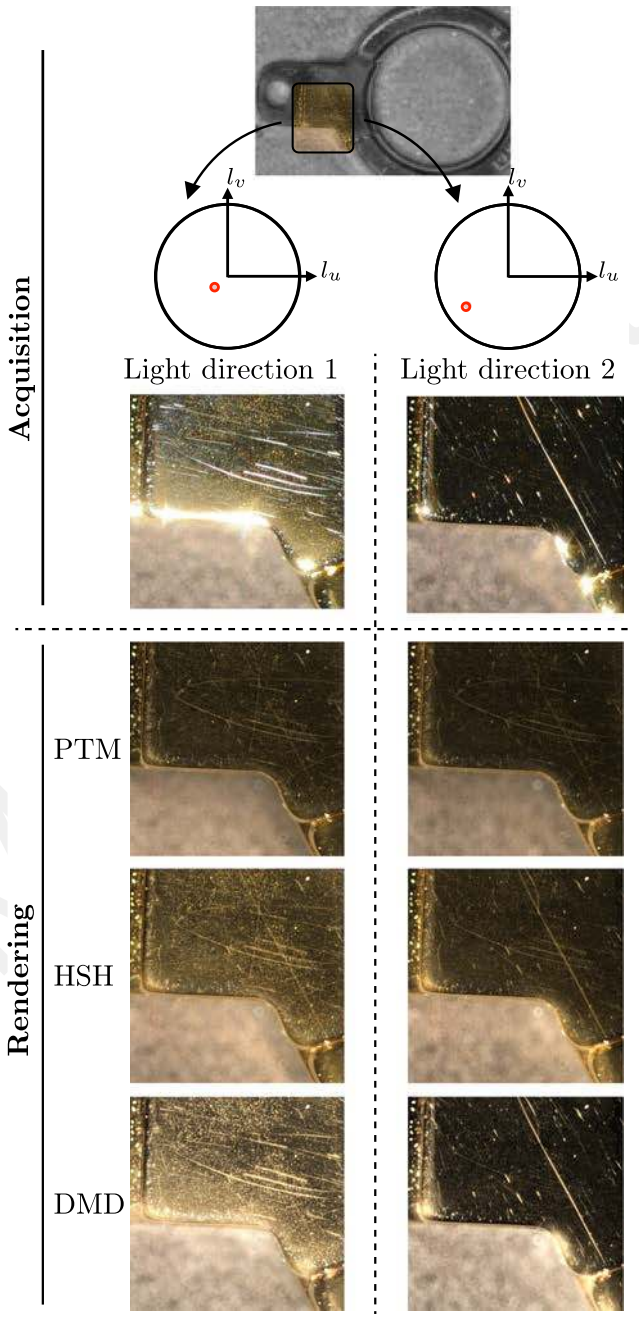

Fig. 8 Cropped views of the acquired and reconstructed images from *Dataset* 1, by the *PTM*, *HSH* and *DMD* methods, in two directions of illumination

DMD for a pixel extracted from the sample *Dataset 1*, points indicated by a circle marker represent the measured luminance ($\mathcal{G}$) for this pixel. We can clearly notice that the points cloud is better approximated by the DMD method, particularly where rapid angular changes in luminance are observed. This quality assessment of the angular reflectance modeling, illustrated for one pixel in Fig. 6, could be extended to all pixels to provide global indicators of the quality of RTI-based reconstructions, on which the following assessment focuses.

One of the main objectives of the implementation of the RTI methods is the modeling of the appearance of the surfaces. However, the process of reconstruction and relighting from any arbitrary direction needs to be fast, particularly for quality inspection. A comparative analysis of visual renderings obtained by RTI methods is carried out in order to show the advantages of the modal approach in comparison with the two other commonly used reconstruction methods.

Figures 7, 8, 9 and 11 show the results for local and global reconstructions associated with directions of acquisition defined in the coordinate system (l_u, l_v) (dome of light viewed from above) for sets of stereo photometric images associated to *Dataset 1–3*. Results depict that the three reconstruction methods described previously provide photo-realistic visual renderings. By estimating the angular reflectance of the pixels separately, the quality of reconstructions is not impaired and does not generate high-frequency noise. Hence, it is unnecessary to accommodate interpixel

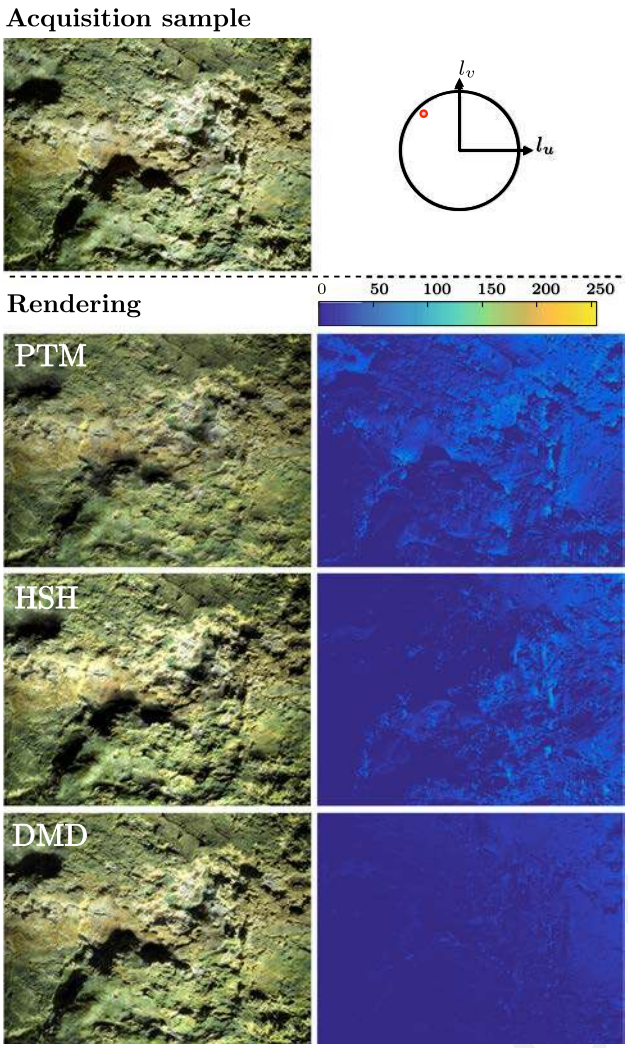

Fig. 9 Cropped view of the acquired and reconstructed images from *Dataset* 2, in a single direction of illumination, by the *PTM*, *HSH* and *DMD* methods (*left-side*), with the associated error maps (*right-side*)

couplings during reconstruction from RTI data. This can be attributed to the fact that for each pixel, unlike contact measuring instruments, the CCD photosensitive area behaves as a physical integrator of the light irradiating each pixel and its neighbors.

On the results associated with the *Dataset 1* (ring of jewelry), perceptible differences between reconstructions are observable especially where phenomena of high variations of intensity (shadows and specularities) and rapid changes of luminance (e.g., scratches) happen, as illustrated in Figs. 7 and 8. Indeed, the global view of the ring in Fig. 7 and the error maps resulting from the difference between the acquired image and the reconstructed image show that a more accurate approximation of the specular regions and more generally of local areas of shiny surfaces is obtained by the DMD approach. PTM tends to strongly transform the measured reflectances by a smoothed continuous behavior (near-Lambertian), thereby removing the salient features of reflection observed on real surfaces, while HSH and especially DMD allow to reconstruct in a more faithful way the reflectance shapes. From these faithful reconstruction, the visual rendering is better and capture even small details. These visual assessments are confirmed by distance metrics and statistical evaluations, developed later in this section.

Figure 8 shows a local view of the images reconstructed from the ring for two light directions corresponding, respectively, to a normal incidence and a near-grazing incidence. These lighting configurations reveal different scratches over the same region of interest. This phenomenon is well known in sensory inspection. The specular lobes caused by fine scratches form a narrow angular region around the specular direction. It leads to a rapid variation in angular reflectances and a strong contrast with neighbor points showing a Lambertian behavior. Moreover, the scratches on the surface of many objects are much smaller than the size of the optical elements in the system (human eye or sensors in camera), yet the effects they induce in their interactions with light play an important role and could easily and quickly be observed by sampling the surface under different lighting conditions by moving it around. It is noticeable that these scratches are less discernible on images reconstructed by the PTM and HSH methods, which confirms the effect of smoothing expected from these approximation methods. This is due to the low complexity of elementary shapes used for the decomposition of measured reflectances (Fig. 4). On the other side, the reconstructed renderings by the DMD method reproduce faithfully the visual effects of these surface defects.

Figure 9 presents a local view of the wall painting of Germolles for a particular lighting configuration. For this lighting configuration, only the HSH and DMD methods provide equivalent results because the light from the surface is mostly diffused (Lambertian) unlike the shiny surface of the ring of jewelry. However, there is a more realistic reconstruction of the shadows by the DMD approach. In addition the smoothing effect caused by the PTM approach tends to darken the surface appearance, accentuating a matt rendering of the surface than original images. In order to allow a comparison at a glance, a view of PTM and DMD reconstructions (zoom-in) has been superimposed in Fig. 10. This Figure clearly highlights the quality of the DMD reconstruction that offers the recovery of the complete 3D texture relief.

Previous observations regarding the performance of the DMD method are also confirmed on the third dataset (Fig. 11) representing the unidirectional pattern of a gauge block. The parallelism of the unidirectional brushed pattern is one of the best qualities in gauge block. The visual appearance of this repetitive geometric texture is highly dependent on the viewing and lighting configurations making undesired variations (micro-scratches, pits and marks) immediately apparent on the surface when these are not in the predominant direction

Fig. 10 Reconstruction of the wall painting appearance from *Dataset* 2 (Zoom-in)—PTM (*left-side*) versus DMD (*right-side*)

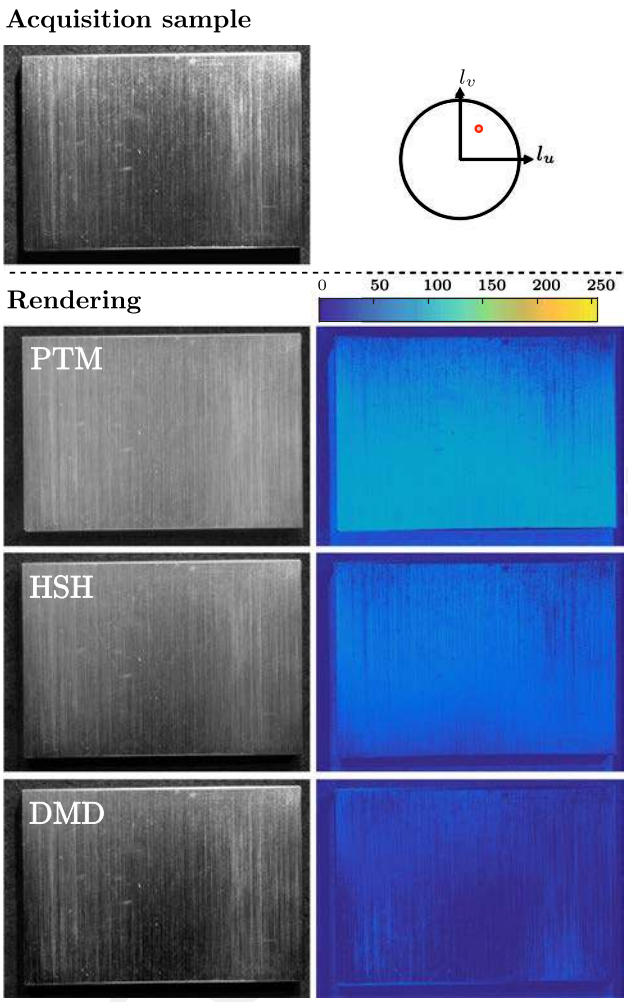

Fig. 11 Macroscopic view of the acquired and reconstructed images from *Dataset* 3, in a single direction of illumination, by the *PTM*, *HSH* and *DMD* methods (*left-side*), with the associated error maps (*right-side*)

of the surface pattern. Moreover, the metal cutting operations or damaged toolings may make deeper lines in the repetitive structural pattern which are perceived brighter than its immediate surround region. These particular textural defects are visually better reproduced by DMD than the two other methods, and a clear difference is observed between the associated error maps.

The histograms in Fig. 12 show the distributions of mean absolute errors of gray level, between the reference image, associated with each lighting acquisition configuration, and the reconstructed images using (a) PTM, (b) HSH and (c) DMD methods, from photometric stereo images for all datasets. Results with the DMD method depict a decrease in the average difference of luminance (approximately -50 and -30% with, respectively, methods PTM and HSH). This result indicates that the clouds of discrete points of luminance are on average better approximated by the implementation of the modal parametrization. This trend is similar for standard deviation assessments. In terms of reconstruction (relighting), these results on *Datasets* 1–3 confirm that the implementation of the DMD approach fit better the original data and, therefore, provides the real visual behavior of studied surfaces.

5.3 Local and pixel-wise comparison

In addition to the visual assessment through relighting, an objective evaluation is performed (pixel-to-pixel and by pixel-to-neighborhood) in order to identify more in detail the effects induced by DMD method compared to PTM and HSH. At this aim, we compare, with two criteria, images obtained after the parametrization (PTM, HSH and DMD) for a particular lighting direction with the image corresponding to the same lighting direction in the set of acquired images. The first criterion is the Peak Signal-Noise Ratio (PSNR), expressed in terms of the logarithmic decibel scale, between two images. A significant drawback of PSNR is that it relies strictly on numeric comparison and does not actually take into account spatial information nor any of the human vision system (HVS) properties [56]. Hence, we use a second criterion of a measure of similarity between images, called Structural SIMilarity (SSIM), which includes this type of weighting [57,58]. SSIM exploits the known characteristics of HVS. Practically, SSIM consists in measuring the structural similarity between two images, based on a combination of luminance, contrast and structure components calculated in sliding windows over the image.

The results for these two criteria applied to the *Dataset* 1 are presented in Fig. 13, in terms of number of descriptors used for angular reflectance reconstruction. The box plots synthesize statistical characteristics (median, quartiles, minimum, maximum) of the values of PSNR and SSIM obtained for all images that result from RTI processing. These results seem to provide a fair compromise between the cost of reconstruction (i.e., the number of descriptors used) and the quality of the reconstruction when using 16 descriptors (asymptotic expansion). Moreover, for a number of descriptors higher than or equal to 16, there is a significant gain in reconstruction

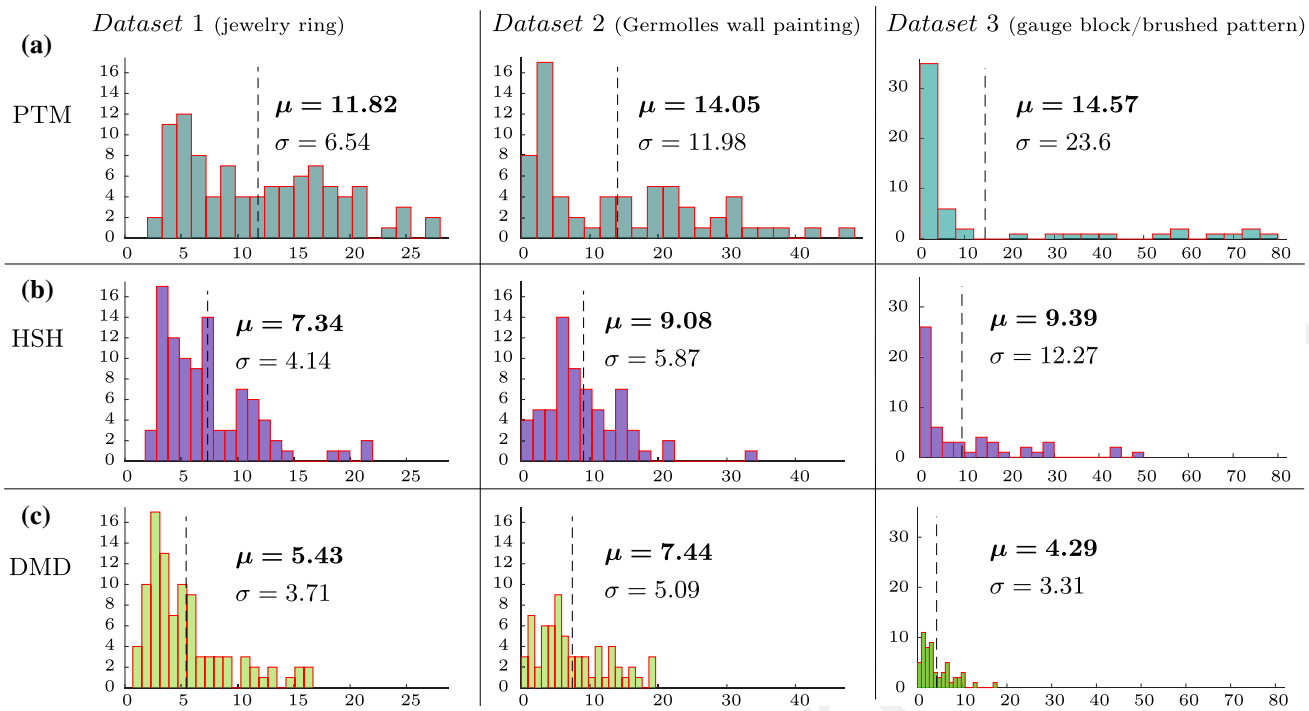

Fig. 12 Distribution of mean absolute errors of gray level (i.e., luminance value) between acquired and reconstructed images of *Datasets* 1–3, in using **a** PTM **b** HSH, and **c** DMD

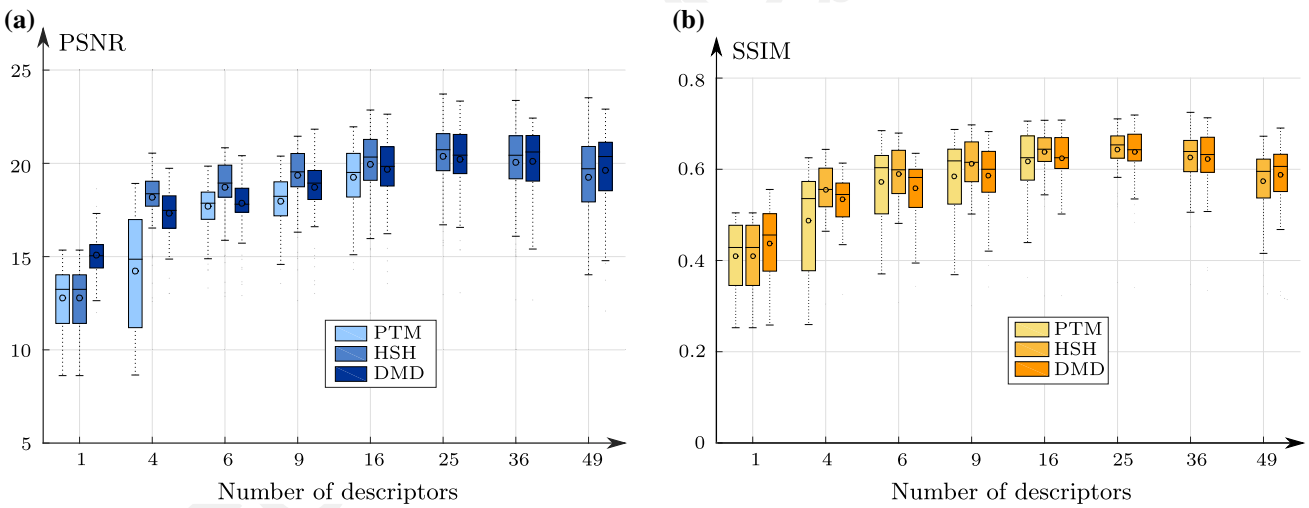

Fig. 13 Comparison of RTI quality based on **a** PSNR and **b** SSIM values, versus the number of descriptors used for reconstruction, for *Dataset 1*

quality using the HSH and DMD method, compared to the results obtained by the PTM method in its original embodiment (6 descriptors). However, significant differences are not statistically conclusive between the HSH and DMD methods, notably when the number of decomposition descriptors is large. Equivalent results are obtained for *Datasets* $2-3$.

Although calculated locally, the obtained results express globally an averaging process (over local differences and inter-configurations of acquisition). This double averaging operation therefore disrupts the relevance of the data obtained by these criteria, in the case of our study. Therefore, it is more interesting to figure out a measure that captures singular behaviors (related to the phenomena of shadow and specularity for example) rather than average one. Indeed, atypical reflectance behaviors are often associated to most salient features (like surface defects) that are naturally rare on surfaces and, therefore, have little influence on the average PSNR and SSIM. However, highlighting and comparing these reconstruction methods, particularly for these atypical

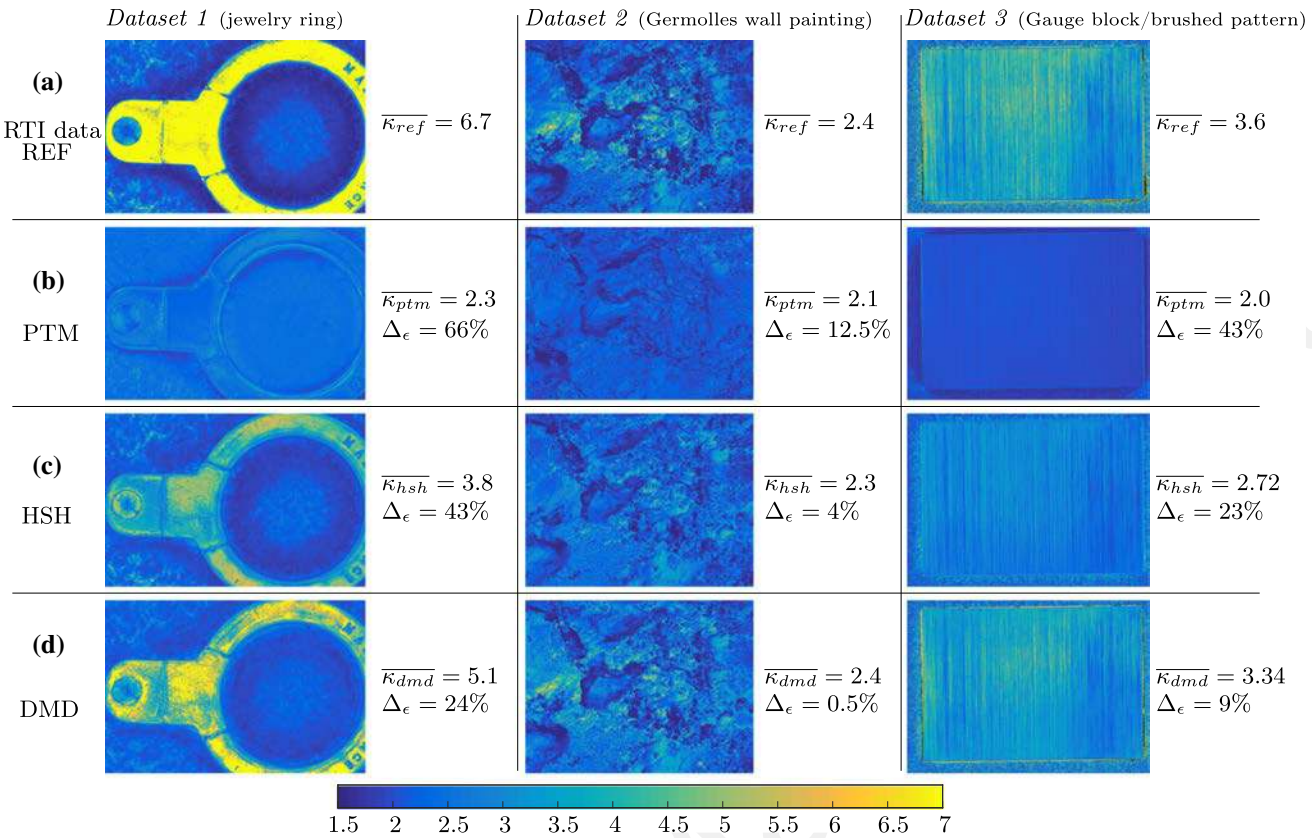

Fig. 14 Kurtosis maps of *Datasets* 1–3. **a** RTI data REF, **b** PTM and **c** HSH, **d** DMD

points, is possible by the construction of maps of local differences.

5.4 Comparison of shape from luminance distributions

The human visual system collects and processes contrast changes of the 2-D image of a surface. Human subjects judgements, while evaluating appearance of surfaces, are also highly correlated with certain image statistics (Kurtosis, Skewness, etc.), measured through psychophysical experiments [59,60]. One of the most influential parameters on the human perception (and subsequent statistics) is the variation of the lighting direction. Therefore, the analysis of the statistics of these variations is thus important to understand the nature of the RTI model transformations and how they affect the estimation of the surface reflectance properties. An analysis of the shape of the distribution of luminance, for each RTI acquisition pixel, is therefore performed in order to assess the differences between reconstructed luminance distribution and measured luminance distribution of *Dataset 1–3* along the dimension associated to illumination direction changes. The shape of the distribution is determined using Skewness and Kurtosis measures based, respectively, on moments of order 3 and of order 4 of luminance distribution. Kurtosis is a measure of the pointedness of the distribution while Skewness is a measure of the asymmetry of the distribution.

Kurtosis of the acquired image data seem to be correlated with the types of reflection. Indeed, the Kurtosis map of *Dataset* 1 estimated from acquired images (Fig. 14) shows a segmentation of diffuse and specular pixels: the specular surface of the object in yellow, the diffuse background in blue and shadows at the edge of the ring in dark blue. Regions in yellow have a Kurtosis higher than 3, implying a more pointed distribution than normal (mesokurtic distribution), whereas the bluest regions with Kurtosis less than 3 indicate a relatively flat distribution (platikurtic distributions). There are few yellow regions on the map associated to the wall painting, thereby confirming the essentially diffuse behavior of this surface. A visual comparison between the maps of Kurtosis shows a clear improvement in the shape measure using the DMD approach for the three datasets. The absolute percentage error Δ_ϵ is computed from the average values of Kurtosis measures ($\overline{\kappa}$) of pixels that belong to the object itself. The reconstruction error in Kurtosis map for *Dataset 1* is significantly less important with DMD (24%) compared to HSH (43%) and PTM (66%). Similar results are obtained for the maps of Skewness (not presented here).

Due to the shape complexity of the descriptors used in the decomposition, HSH and, a fortiori, DMD offer a more

accurate approximation of non-Lambertian behaviors of real surfaces. It leads to a better description of the variations of the luminances, to which the human visual system is particulary sensitive when the incidence of illumination varies on the surface. Skewness and Kurtosis measures permit to highlight the limits of the PTM technique which tends to oversmooth the measured reflectances and generates uniform luminance distributions, thereby removing observable salient features in reflectance space which could facilitate the isolation and identification of surface artifacts.

6 Conclusion

In this article, we have proposed an adaptive and efficient approach to model the angular component of the reflectance from RTI data, based on a parametrization named Discrete Modal Decomposition. The relevance of the DMD approach is studied by comparing the results with those obtained by the two most commonly used RTI methods, which are, respectively, associated to the second-order polynomials (PTM) and a set of hemispherical harmonic functions (HSH). It appears to provide a robust and reliable estimation of the complex local reflectances in terms of both angular variations and the intensity of luminance. If equivalent results are obtained for the diffuse reflectance (Lambertian behavior), a more accurate approximation of the specular lobes, and more generally of local areas of shiny surfaces is provided by this approach.

DMD is therefore particularly relevant for the description of the local angular reflectance surfaces in the context of the issue of detection and characterization of surface defects. It opens up promising prospects in the context of industrial application for surface quality inspection. Applying the presented method to actual experimental measurements, in cultural heritage or industrial applications, could help to better understand the correlations between roughness and reflectance properties, and between these reflectance properties and the visual perception of surfaces. This is the main perspective of the study.

Acknowledgements This work was supported by the partners of the *MeSurA* project (Measuring Surface Appearance): the centre technique de l'industrie et du décolletage (CETIM-CTDEC), the centre technique du comité Francéclat (CETEHOR), the société OPTO France, and the conseil départemental de Haute-Savoie. Authors would also like to thank the cultural and scientific project at Château de Germolles, supported by DRAC-Bourgogne and EU COST Action TD 1201, COSCH (http://www.cosch.info).

References

1. Béland, M.-C., Bennett, J.M.: Effect of local microroughness on the gloss uniformity of printed paper surfaces. Appl. Opt. **39**, 2719–2726 (2000)
2. Simonot, L., Elias, M.: Color change due to surface state modification. Color Res. Appl. **28**(1), 45–49 (2002)
3. Briones, V., Aguilera, J.M., Brown, C.A.: Effect of surface topography on color and gloss of chocolate samples. J. Food Eng. **77**(4), 776–783 (2006)
4. Le Goïc, G., Bigerelle, M., Samper, S., Favreliere, H., Pillet, M.: Multiscale roughness analysis of engineering surfaces: a comparison of methods for the investigation of functional correlations. Mech. Syst. Signal Process. **66**, 437–457 (2016)
5. Nicodemus, F.E.: Directional reflectance and emissivity of an opaque surface. Appl. Opt. **4**(7), 1–8 (1965)
6. Nicodemus, F.E., Richmond, J.C., Hsia, J.J., Ginsberg, I.W., Limperis, T.: Geometrical considerations and nomenclature for Reflectance. Institute for Basic Standards, National Bureau of Standards, Washington (1977)
7. Dana, K.J., van Ginneken, B., Nayar, S.K., Koenderink, J.J.: Reflectance and texture of real-world surfaces. ACM Trans. Graph. **18**(1), 1–34 (1999)
8. Müller, G., Meseth, J., Sattler, M., Sarlette, R., Klein, R.: Acquisition, synthesis, and rendering of bidirectional texture functions. Comput. Graph. Forum **24**, 83–109 (2005)
9. Filip, J., Haindl, M.: Bidirectional texture function modeling: a state of the art survey. IEEE Trans. Pattern Anal. Mach. Intell. **31**(11), 1921–1940 (2009)
10. Malzbender, T., Gelb, D., Wolters, H.: Polynomial texture maps. In: Proceedings of the 28th Annual Conference on Computer Graphics and Interactive Techniques, pp. 519–528 (2001)
11. Malzbender, T., Gelb, D.G.: Apparatus for and method of enhancing shape perception with parametric texture maps. US Patent Office (2000)
12. Malzbender, T.: Direction-dependent texture maps in a graphics system. US Patent Office (2001)
13. Malassiotis, S., Strintzis, M.G.: Stereo vision system for precision dimensional inspection of 3D holes. Mach. Vis. Appl. **15**(2), 101–113 (2003)
14. Angelopoulou, M.E., Petrou, M.: Evaluating the effect of diffuse light on photometric stereo reconstruction. Mach. Vis. Appl. **25**(1), 199–210 (2014)
15. Gautron, P., Krivanek, J., Pattanaik, S.N., Bouatouch, K.: A novel hemispherical basis for accurate and efficient rendering. In: Eurographics Symposium on Rendering 2004 (2004)
16. Westin, S.H., Arvo, J.R., Torrance, K.E.: Predicting reflectance functions from complex surfaces. Ph.D. thesis, Faculty of the Graduate School of Cornell University, New York, USA (1992)
17. MacDonald, L.W.: Colour and directionality in surface reflectance. In: Proc. Conf. on Artificial Intelligence and the Simulation of Behaviour (AISB) (2014)
18. Murray-Coleman, J.F., Smith, A.M.: The automated measurement of BRDFs and their application to luminaire modeling. J. Illum. Eng. Soc. **19**(1), 87–99 (1990)
19. Obein, G., Ouarets, S., Ged, G.: Evaluation of the shape of the specular peak for high glossy surfaces. IS&T/SPIE Electron. Imaging **9018**, 901805 (2014)
20. Le Breton, R., Ged, G., Obein, G.: Out of plane BRDF measurement at LNE-CNAM using Condor, our primary goniospectrophotometer. In: Proceedings of the 28th Session of the CIE (Manchester), pp. 1401–1407 (2015)
21. Blinn, J.F.: Models of light reflection for computer synthesized pictures. ACM SIGGRAPH Comput. Graph. **11**, 192–198 (1977)
22. Lafortune, E.P.F., Foo, S.-C., Torrance, K.E., Greenberg, D. P.: Non-linear approximation of reflectance functions. In: Proceedings of the 24th Annual Conference on Computer Graphics and Interactive Techniques (1997)
23. Ward, G.J., Ward, G.J.: Measuring and modeling anisotropic reflection. ACM SIGGRAPH Comput. Graph. **26**, 265–272 (1992)

24. Schröder, P., Sweldens, W.: Spherical wavelets: texture processing. In: Rendering Techniques' 95, pp. 252–263. Springer, Vienna (1995)
25. Koenderink, J.J., van Doorn, A.J., Stavridi, M.: Bidirectional reflection distribution function expressed in terms of surface scattering modes. In: Computer Vision—ECCV '96, Berlin. Springer, Berlin (1996)
26. Cook, R.L., Torrance, K.E.: A reflectance model for computer graphics. ACM Trans. Graph. (TOG) **1**, 7–24 (1982)
27. Oren, M., Nayar, S. K.: Generalization of Lambert's reflectance model. In: Proceedings of the 21st Annual Conference on Computer Graphics and Interactive Techniques, pp. 239–246 (1994)
28. Beckmann, P., Spizzichino, A.: The Scattering of Electromagnetic Waves from Rough Surfaces. Artech House on Demand, London (1987)
29. He, X.D., Torrance, K.E., Sillion, F.X., Greenberg, D.P.: A comprehensive physical model for light reflection. ACM SIGGRAPH Comput. Graph. **25**, 175–186 (1991)
30. Kotani, K., Tachino, R., Terado, I., Kenmochi, Y.: Reflection and transparency model of rose petals for computer graphics based on the micro-scopic scale structures. In: 6th International Conference on Image Processing (ICIP'99), vol. 3, pp. 593–596. IEEE (1999)
31. Berthier, S.: Photonique des Morphos. Springer, Paris (2010)
32. Veach, E., Guibas, L.J.: Metropolis Light Transport. ACM Press/Addison-Wesley Publishing Co., New York (1997)
33. Jensen, H.W., Marschner, S.R., Levoy, M., Hanrahan, P.: A Practical Model for Subsurface Light Transport. ACM, New York (2001)
34. Wang, J., Dong, Y., Tong, X., Lin, Z., Guo, B., Wang, J., Dong, Y., Tong, X., Lin, Z., Guo, B.: Kernel Nyström Method for Light Transport, vol. 28. ACM, New York (2009)
35. MacDonald, L.W.: Visualising an Egyptian artefact in 3D: comparing RTI with laser scanning. In: Proceedings of the 2011 International Conference on Electronic Visualisation and the Arts EVA'11 (2011)
36. Zhang, M., Drew, M.S.: Efficient robust image interpolation and surface properties using polynomial texture mapping. EURASIP J. Image Video Process. **2014**(1), 1–19 (2014)
37. Drew, M.S., Hajari, N., Hel-Or, Y., Malzbender, T.: Specularity and Shadow Interpolation via Robust Polynomial Texture Maps, pp. 114.1–114.11. Citeseer, London (2009)
38. Proença, A.J.: RTI-based techniques and tools for digital surrogates. Ph.D. thesis, Université du Minho (Portugal) (2009)
39. Earl, G., Martinez, K.: Archaeological applications of polynomial texture mapping: analysis, conservation and representation. J. Archaeol. Sci. **37**(8), 2040–2050 (2010)
40. Duffy, S.B.: Multi-Light Imaging for Heritage Applications. English Heritage, Swindon (2013)
41. Newman, S.E.: Applications of reflectance transformation imaging (RTI) to the study of bone surface modifications. J. Archaeol. Sci. **53**, 536–549 (2015)
42. Durou, J.D.: Shape from shading—Eclairages, réflexions et perspectives. Rapport d'Habilitation à Diriger des Recherches (2007)
43. Raj, A., Adelson, E.H., Johnson, M.K., Cole, F.: Microgeometry Capture Using an Elastomeric Sensor. ACM, New York (2011)
44. Malzbender, T., Gelb, D.: Polynomial Texture Map (. ptm) File Format. Tech. rep., Hewlett-Packard (2001)
45. Kautz, J., Sloan, P.P., Snyder, J.: Fast, arbitrary BRDF shading for low-frequency lighting using spherical harmonics. In: Proceedings of the 13th Eurographics Workshop on Rendering (2002)
46. Mudge, M., Malzbender, T., Chalmers, A., Scopigno, R.: Image-based empirical information acquisition, scientific reliability, and long-term digital preservation for the natural sciences and cultural heritage. In: Eurographics, (Crete), pp. 2040–2050 (2008)
47. Krivanek, J., Ferwerda, J.A., Bala, K.: Effects of global illumination approximations on material appearance. ACM Trans. Graph. (TOG) **29**(4), 1 (2010)
48. Palma, G., Corsini, M., Cignoni, P.: Dynamic shading enhancement for reflectance transformation imaging. J. Comput. Cult. Herit. **3**, 6 (2010)
49. Favreliere, H.: Modal tolerancing : from metrology to specifications. Ph.D. thesis, Annecy (2009)
50. Samper, S., Adragna, P.A., Favreliere, H.: Modeling of 2d and 3d assemblies taking into account form errors of plane surfaces. J. Comput. Inf. Sci. Eng. **9**(4), 041005 (2009)
51. Le Goïc, G., Favreliere, H., Samper, S., Formosa, F.: Multi scale modal decomposition of primary form, waviness and roughness of surfaces. Scanning **33**(5), 332–341 (2011)
52. Grandjean, J., Le Goic, G., Favreliere, H., Ledoux, Y., Samper, S., Formosa, F., Devun, L., Gradel, T.: Multi-scalar analysis of hip implant components using modal decomposition. Meas. Sci. Technol. **24**(1), 125702 (2012)
53. Pottier, T., Louche, H., Samper, S., Favreliere, H., Toussaint, F., Vacher, P.: A new filtering approach dedicated to heat sources computation from thermal field measurements. In: PhotoMechanics Conference, pp. 1–4 (2013)
54. Pottier, T., Louche, H., Samper, S., Favreliere, H., Toussaint, F., Vacher, P.: Proposition of a modal filtering method to enhance heat source computation within heterogeneous thermomechanical problems. Int. J. Eng. Sci. **81**, 163–176 (2014)
55. Degrigny, C., Piqué, F., Papiashvili, N., Guery, J., Mansouri, A., Le Goïc, G., Detalle, V., Martos-Levif, D., Mounier, A., Wefers, S., Tedeschi, C., Cucchi, M., Vallet, J.-M., Pamart, A., Pinette, M.: Technical study of Germolles' wall paintings: the input of imaging technique. Virtual Archaeol. Rev. **7**, 1–8 (2016)
56. Lorenzetto, G.P.: Image comparison metrics: a review. Tech. rep. (1998)
57. Wang, Z., Bovik, A.C., Simoncelli, E.P.: Structural approaches to image quality assessment. In: Handbook of Image and Video Processing, pp. 961–974. Elsevier (2005)
58. Wang, Z., Bovik, A.C., Sheikh, H.R., Simoncelli, E.P.: Image quality assessment: from error visibility to structural similarity. IEEE Trans. Image Process. **13**, 600–612 (2004)
59. Nishida, S., Shinya, M.: Use of image-based information in judgments of surface-reflectance properties. JOSA A **15**, 2951–2965 (1998)
60. Sharan, L., Li, Y., Motoyoshi, I., Nishida, S., Adelson, E.H.: Image statistics for surface reflectance perception. JOSA A **25**, 846–865 (2008)